THE ASTRONOMICAL JOURNAL, 115:361–372, 1998 January

HIGH-PRECISION ALGORITHMS FOR ASTROMETRY: A COMPARISON OF TWO APPROACHES

GEORGE H. KAPLAN
US Naval Observatory, 3450 Massachusetts Avenue, NW, Washington, DC 20392
Received 1997 August 25

ABSTRACT

This paper discusses the correspondence between two approaches to astrometric observational reductions: the approach based on angular observables used for optical observations, and the approach based on the interferometric delay observable used for very long baseline radio interferometry (VLBI) observations. A procedure is presented by which VLBI algorithms can be used for optical observations. This scheme can help to guarantee consistent treatment of observational results in the two regimes. Differences between angle- and delay-based algorithms in current use are shown to be less than 1 μas. However, the physical models used as the bases for the algorithms must be improved to reach external accuracies at such levels.

Key words: astrometry — catalogs — reference systems — techniques: interferometric

1. INTRODUCTION

This paper discusses some important algorithms used in wide-angle astrometry, defined here as the measurement of the relative positions of celestial objects over angular scales of a radian or more. Typically, a program of wide-angle astrometry results in a catalog of positions (at some epoch) and proper motions (if measurable) of some restricted class of objects. *Fundamental* astrometry is a special form of wide-angle astrometry in which the coordinate system of the final catalog is tied to the celestial equator and the equinox. The discussion in this paper applies to the more general case and is not coordinate system dependent.

Specifically of interest here is the group of algorithms that have become standard in accounting for the physical effects traditionally called annual and diurnal aberration and gravitational light bending. Currently achievable observational accuracies for wide-angle astrometry, of order 1 mas, require that these effects be correctly modeled at a level of parts in 10^6 for aberration and 10^4 for light bending. New observational techniques under development promise to raise the accuracy requirements by several orders of magnitude. These algorithms are important because they must be applied to all wide-angle astrometric measurements, whether ground- or space-based, and regardless of the distance of the objects observed.

The paper discusses the correspondence between two approaches to astrometric observational reductions: the approach based on angular observables used for optical observations, and the approach based on the interferometric delay observable used for very long baseline radio interferometry (VLBI) observations. A procedure is presented by which VLBI algorithms can be used for optical observations. This scheme can help to guarantee consistent treatment of observational results that are often combined or compared. It also allows for the evaluation of the precision of the algorithms.

As used in this paper, *precision* refers to how well a mathematical representation of some effect corresponds to the physical model constructed to account for it. *Accuracy* refers to how well the physical model corresponds to reality. Thus, an algorithm can be precise without being accurate, if, for example, a very exact mathematical development is used to represent a relatively crude physical model. The technique that is the main subject of this paper provides information on the precision of the algorithms involved but not necessarily their accuracy. The accuracy of algorithms is also obviously important, and will be touched on in § 10.

Section 2 provides some background information on high-precision astrometry and the algorithms that support it. Section 3 describes the algorithms used in optical astrometry, while § 4 presents the comparable VLBI algorithms. In § 5, the procedure that allows the two kinds of algorithms to be directly compared is developed. Section 6 describes how the comparison software works, and § 7 presents numerical results from the comparison. Section 8 shows how a modification to an algorithm can be tested by the procedures developed in the paper. Section 9 deals with the large-aperture case, and § 10 provides a summary and conclusion.

2. BACKGROUND

A full discussion of the motivations for high-precision wide-angle astrometry are beyond the scope of this paper, but several recent IAU conferences have covered this subject well; see Lieske & Abalakin (1990), Hughes, Smith, & Kaplan (1991), or Høg & Seidelmann (1995). Suffice it here to say that an important goal of this work has been the construction of high-precision celestial reference frames in various wavelength regimes and the determination of the relationships between these reference frames. The primary astrometric technique in the radio regime is very long baseline interferometry, which now routinely provides large-angle measurements with accuracies of $\sim$1 mas or better (Ma 1990; Jacobs & Sovers 1993; Johnston et al. 1995). In the optical band, the *Hipparcos* satellite has determined stellar positions with similar accuracies (Mignard 1995), and ground-based interferometry may soon be competitive (Hutter, Johnston, & Mozurkewich 1995). Several proposals for space-based observing systems anticipate wide-angle astrometry at the 5–50 μas level (Reasenberg et al. 1988; Lindegren & Perryman 1995; Seidelmann et al. 1995).

Although each astrometric observing program has unique requirements, there are a number of physical and

geometric effects that enter into the data reductions that are common to all techniques. If high-precision reference frames are to be aligned, it would seem desirable to have some assurance that the data have been handled consistently. The International Earth Rotation Service (IERS) has established standard models and algorithms (McCarthy 1992, 1996) that facilitate comparison of data within its field. The IAU Working Group on Astronomical Standards has been tasked with establishing standard astrometric algorithms for the broader community (Fukushima 1995; IAU 1996).

This paper reports on the treatment of the physical effects traditionally referred to as aberration and gravitational light deflection. These names reflect a particular way of conceptualizing these effects, one based on the point of view of an observing system with a single, well-defined location—that is, one with an aperture small compared with the radius of Earth. For such a system, these effects appear as small angular departures from the Euclidean direction of an observed object. Practitioners of VLBI treat these effects quite differently than do other observers, principally because they use a very sparsely filled aperture, each segment of which is separated from the others by distances of thousands of kilometers. The relative motions of the various parts of the total aperture are not negligible. The observable in the VLBI case is the time difference (group delay) between a wave front's arrival at one segment of the aperture and its arrival at another. Although the basic framework for modeling the physical effects that we are considering—special and general relativity—is the same in the two cases, the algorithms used are actually quite different. It is therefore fair to ask to what extent the VLBI treatment is consistent, in practice, with the algorithms used for small apertures.

3. TREATMENT USING ANGLE VARIABLES

The traditional treatment of stellar aberration can be found in any textbook on spherical astronomy, for example, Woolard & Clemence (1966) or Green (1985). Aberration is the effect by which a moving observer sees an apparent angular shift in the position of a fixed light source. Of course, for unaccelerated motion, one can simply shift reference frames so that the observer is at rest and the effect appears as a light-time problem. In the solar system, accelerations are small (spacetime is nearly flat), and such a shift in reference frames can simplify the computations when high precision is not required. For example, in computing the positions of planets as seen from Earth, it was for many years a common practice to combine aberration and light-time effects into "planetary aberration," which is actually based on a light-time perspective (Hohenkerk et al. 1992). For stars, however, the light time is unknown (or considered irrelevant), and it is more convenient to treat them as fixed for this purpose and to adjust their apparent positions for the motion of Earth relative to the solar system barycenter. Hence the name "annual aberration" when the effect is treated from this perspective.

In recent years, high precision has become more important and computational shortcuts unnecessary. Light time and aberration are handled separately, and both computations are carried out using the (assumed inertial) frame of the solar system barycenter. This allows the inclusion of the relativistic deflection of light in the Sun's gravitational field. The computations are properly carried out in the following order: light time, gravitational deflection, aberration. The algorithms effectively follow a photon from a moving source to a moving observer. Thus, the computations implicitly assume a point source and a point observer, both with known coordinates and velocities with respect to the solar system barycenter, in the relativistic metric being used. In practice, the source coordinates are obtained from an ephemeris (for solar system bodies) or from catalog data (for stars and other bodies outside the solar system). The entire procedure is described by Kaplan et al. (1989) and Hohenkerk et al. (1992), and summarized below; the formulae for gravitational deflection and relativistic aberration are based on the developments of Murray (1983; for an independent derivation, see Soffel 1989). Refraction due to Earth's atmosphere is ignored.

The following notation will be used: The vectors $\boldsymbol{K}$, $\boldsymbol{S}$, $\boldsymbol{E}$, and $\boldsymbol{R}$ represent the positions of the observed body (planet or star), Sun, Earth, and observer, respectively, with corresponding unit vectors $\boldsymbol{k}$, $\boldsymbol{s}$, $\boldsymbol{e}$, and $\boldsymbol{r}$. Unsubscripted vectors are relative to an origin at the solar system barycenter; subscripts S, E, and R, when used, denote a coordinate origin at the Sun, Earth, and observer, respectively. Unless otherwise noted, these vectors all apply to the (coordinate) time of observation t. Isotropic coordinates are assumed. The vector $\boldsymbol{R}$ can be considered to be the sum of Earth's barycentric position vector and the observer's geocentric position vector: $\boldsymbol{R} = \boldsymbol{E} + \boldsymbol{R}_{\rm E}$.

The geometric (Euclidean) position of the object with respect to the observer is $\boldsymbol{K}_R = \boldsymbol{K} - \boldsymbol{R}$, where both $\boldsymbol{K}$ and $\boldsymbol{R}$ are evaluated at time t. The corresponding unit vector in the geometric direction of the object is $\boldsymbol{k}_R$. A first approximation to the light time, Δt, between a solar system object and the observer is given by $\Delta t = |\boldsymbol{K}_R|/c$. Adjusting the position vector of the observed planet for light time is then accomplished by iteratively evaluating the two formulae $\boldsymbol{K}'_R = \boldsymbol{K}(t - \Delta t) - \boldsymbol{R}(t)$ and $\Delta t = |\boldsymbol{K}'_R|/c$ until convergence. The vector $\boldsymbol{K}'_R$ is then the position of the planet relative to the observer, accounting for light time—that is, it is the vector connecting the observer at time t (light arrival) with the observed planet at time $t - \Delta t$ (light departure). This pair of formulae applies only to angular measurements; it is too simple for ranging measurements, which are two-way and require an additional relativistic term. The neglected term accounts for the "Shapiro delay," the extra light time due to the Sun's gravitational field (Shapiro 1964), which affects the angular coordinates of the planets only at the microarcsecond level, and then only near the solar limb.

For stars or other bodies outside the solar system, the light time and its time derivative are assumed to be irrelevant and are not computed. More specifically, they are assumed to be implicitly included in the catalog quantities. That is, for stars, $\boldsymbol{K}'_R = \boldsymbol{K}_R = \boldsymbol{K}(t) - \boldsymbol{R}(t)$, where $\boldsymbol{K}(t)$ is the geometric position vector of the star, with respect to the solar system barycenter, at the epoch of observation, calculated from the catalog position, proper motion, parallax, and radial velocity. In the stellar case, then, $\boldsymbol{k}'_R = \boldsymbol{k}_R$. For objects effectively at infinity (parallax unmeasurable), $\boldsymbol{k}'_R = \boldsymbol{k}_R = \boldsymbol{k}_{\rm E} = \boldsymbol{k}_{\rm S} = \boldsymbol{k}$.

To compute the relativistic deflection of light in the Sun's gravitational field, we will define the vectors $\boldsymbol{R}_{\rm S} = \boldsymbol{R} - \boldsymbol{S}$, representing the heliocentric position of the observer, and $\boldsymbol{K}'_{\rm S} = \boldsymbol{K}'_R + \boldsymbol{R}_{\rm S}$, the heliocentric position of the observed body, corrected for light time to the observer. The unit vectors $\boldsymbol{k}'_R$, $\boldsymbol{k}'_{\rm S}$, and $\boldsymbol{r}_{\rm S}$ correspond to the position vectors $\boldsymbol{K}'_R$,

$\boldsymbol{K}'_S$, and $\boldsymbol{R}_S$; the quantity R_S represents the magnitude of $\boldsymbol{R}_S$, the distance of the observer from the Sun. Then the unit vector $\boldsymbol{k}''_R$, representing the apparent direction of the body seen by the observer, accounting for both light time and gravitational deflection, is given by

$$\boldsymbol{k}''_R = \boldsymbol{k}'_R + \frac{2GM_\odot}{c^2 R_S} \frac{(\boldsymbol{k}'_R \cdot \boldsymbol{k}'_S)\boldsymbol{r}_S - (\boldsymbol{r}_S \cdot \boldsymbol{k}'_R)\boldsymbol{k}'_S}{1 + \boldsymbol{k}'_S \cdot \boldsymbol{r}_S}, \quad (1)$$

where G is the gravitational constant, $M_\odot$ is the mass of the Sun, and c is the speed of light. The apparent angular deflection seen by the observer is radially outward from the Sun. A spherical gravitational field has been assumed. The magnitude of the angular deflection given by equation (1) is $\Delta\phi = g \tan(\psi/2)$, where $g = 2GM_\odot/c^2 R_S \approx 4$ mas and ψ is the *heliocentric* angle between the directions of Earth and the observed body. As noted by Shapiro (1967), this relation is odd in that it does not depend on the distance of the body observed. With the appropriate change of variables, equation (1) can be easily applied to gravitating bodies other than the Sun (including Earth itself), and the total deflection can be approximated to high accuracy by the sum of the individual deflections.

Aberration can be computed as follows: Let $\dot{\boldsymbol{R}}$ be the velocity vector (speed $\dot{R}$) of the observer with respect to the solar system barycenter. The unit vector in the apparent direction of the body, as seen by the observer, adjusted for light time, gravitational deflection, and aberration, is

$$\boldsymbol{k}'''_R = \langle \eta \boldsymbol{k}''_R + \kappa \dot{\boldsymbol{R}}/c \rangle , \quad (2)$$

where the angle brackets imply normalization (to unit length). Classically, $\eta = \kappa = 1$. Since the barycentric velocity of the observer $\dot{\boldsymbol{R}}$ is the sum of the barycentric velocity of Earth and the geocentric velocity of the observer, both annual and diurnal aberration have been included. For Earth-based observers the classical formula is good to about 0.5 mas, quite adequate for most applications. When the aberration formula is developed using a Lorentz transformation, we have

$$\beta = \dot{R}/c , \quad \gamma = 1/\sqrt{1 - \beta^2} ,$$

$$\cos\theta = \boldsymbol{k}''_R \cdot \dot{\boldsymbol{R}}/\dot{R} ,$$

$$\eta = \gamma^{-1}/(1 + \beta\cos\theta) ,$$

$$\kappa = \left(1 + \frac{\beta\cos\theta}{1 + \gamma^{-1}}\right) \Big/ (1 + \beta\cos\theta) . \quad (3)$$

The apparent angular deflection of the observed body's direction is toward the direction of the observer's motion and is independent of the object's distance. The magnitude of the deflection is approximately $\Delta\theta = (\dot{R}/c)\sin\theta$, where θ is the angle, at the observer, between the direction of motion and the direction of the observed body (as defined by $\boldsymbol{k}''_R$). For observers on Earth, $\dot{R}/c \approx 10^{-4} \approx 21''$.

The unit vector $\boldsymbol{k}'''_R$ defines the "apparent place" of the planet or star; if there were no atmospheric refraction, it would define the point on the sky where the object would appear to be. The above formulae, or their equivalents, have come into widespread use. For example, the SLALIB (Wallace 1994) and NOVAS (Kaplan 1990) astrometry software packages implement them, and they have been used for the reduction of the *Hipparcos* satellite observations (Lindegren et al. 1992). They are also used for the preparation of Apparent Places of Fundamental Stars (see Lederle & Schwan 1984) and the Astronomical Almanac (see pp. B36–B41). Although more accurate formulae have been developed (e.g., Richter & Matzner 1982; Klioner & Kopejkin 1992), these have not yet come into general use; the next generation of astrometric satellites may require the use of the more complex developments. It should be noted that, for satellite astrometry, the computation of aberration to 1 μas would require a determination of the satellite's velocity vector to 1.5 mm s^{-1}, a technical challenge.

4. TREATMENT USING VLBI DELAY

For interferometers capable of making astrometric measurements, the observable is the difference in arrival times of a wave front at two receiving stations (telescopes, siderostats, or antennas). For connected-element interferometers, the time difference, τ, is often estimated in the following way: First, the star's apparent place in the sky, represented by the unit vector $\boldsymbol{k}'''_R$, is computed as in § 3. (Again, we are ignoring the refraction of Earth's atmosphere.) For this calculation, one has to choose coordinates for the location of the observer, so a point somewhere on the baseline connecting the two stations, the "phase center" of the interferometer, is used. Once the apparent place is computed, in some celestial coordinate system, the baseline vector is transformed via a series of rotations to the same system; it becomes the vector $\boldsymbol{B}(t)$, which rotates with Earth. The instantaneous delay, τ, is then simply $\tau = -\boldsymbol{B}(t) \cdot \boldsymbol{k}'''_R/c$ if both the baseline $\boldsymbol{B}$ and delay τ are defined in the same sense, e.g., station 2 minus station 1. Note that the measured delay divided by the length of the baseline in light time is simply the direction cosine of the apparent stellar direction with respect to the instantaneous baseline direction.

It may not be immediately obvious that this approach remains valid as the length of the interferometer baseline increases. At some level of accuracy, and for some baseline lengths, it would seem that we should account for the fact that the two stations are actually in two different reference frames. The VLBI community deals with station separations of many thousands of kilometers, and the computation of VLBI delay has always been performed entirely in the time domain. The apparent place of the source is not used. Aberration is replaced in this paradigm by the "retarded baseline" effect, which is the motion of the second antenna after the wave front passes the first antenna but before it reaches the second. The gravitational deflection of light appears as the differential Shapiro delay—a small difference in the gravitational retardation of the wave front at the two antennas due to the slightly different paths through the solar system.

There have been a number of developments of the VLBI delay observable, for example, by Robertson (1975), Hellings (1986), Zhu & Groten (1991), Shapiro (reported in Ryan 1991), Shahid-Saless, Hellings, & Ashby (1991), and Soffel et al. (1991). A consensus model for use in geodetic-astrometric VLBI experiments emerged from a workshop held in 1990 (Eubanks 1991a). We will continue to use the notation introduced in § 3. The wave front arrival times at stations 1 and 2 are t_1 and t_2, and the delay is then $\tau = t_2 - t_1$. If we use (barycentric) position vectors $\boldsymbol{R}_1$ and $\boldsymbol{R}_2$ for stations 1 and 2, respectively, then the baseline vector that connects the stations at time t_1 is $\boldsymbol{B}(t_1) = \boldsymbol{R}_2(t_1) - \boldsymbol{R}_1(t_1)$. The consensus model for the delay for an infinitely distant

object, as presented in the standards documents of the IERS (McCarthy 1992, 1996), expressed in our notation, is

$$\tau_{\rm E} = \left\{ \Delta t_g - \frac{\boldsymbol{k}\cdot\boldsymbol{B}(t_1)}{c} \times \left[1 - (1+\gamma)U - \frac{1}{c^2}\left(\frac{\dot{\boldsymbol{E}}^2}{2} - \dot{\boldsymbol{E}}\cdot\dot{\boldsymbol{R}}_{2_{\rm E}} \right) \right] - \frac{\dot{\boldsymbol{E}}\cdot\boldsymbol{B}(t_1)}{c^2}\left(1 + \frac{\boldsymbol{k}\cdot\dot{\boldsymbol{E}}}{2c} \right) \right\} \Bigg/ \left[1 + \frac{\boldsymbol{k}}{c}\cdot(\dot{\boldsymbol{E}} + \dot{\boldsymbol{R}}_{2_{\rm E}}) \right], \quad (4)$$

where the quantities on the right-hand side are all evaluated at time t_1. This equation holds for observed objects effectively at infinity (far outside the solar system). The delay, $\tau_{\rm E}$, is expressed in a *geocentric* coordinate time such as TAI (hence the subscript). The vector $\dot{\boldsymbol{E}}$ is the velocity of the geocenter with respect to the solar system barycenter; $\boldsymbol{k}$ is the unit vector in the geometric direction of the object (for objects at infinity $\boldsymbol{k} = \boldsymbol{k}_{\rm S} = \boldsymbol{k}_{\rm E} = \boldsymbol{k}_{R_1} = \boldsymbol{k}_{R_2}$); $\dot{\boldsymbol{R}}_{2_{\rm E}}$ is the geocentric velocity of the second antenna; U is the total gravitational potential at the geocenter; and γ is a parameterized post-Newtonian (PPN) parameter ($\gamma = 1$ in general relativity). Note that the vector sum $\dot{\boldsymbol{E}} + \dot{\boldsymbol{R}}_{2_{\rm E}}$ in the denominator is equal to the barycentric velocity of station 2. The quantity Δt_g is the differential gravitational delay, calculated for the Sun's field using

$$\Delta t_g = (1+\gamma)\frac{GM_\odot}{c^3}\ln\left(\frac{\boldsymbol{k}\cdot\boldsymbol{R}_{1_{\rm S}} + |\boldsymbol{R}_{1_{\rm S}}|}{\boldsymbol{k}\cdot\boldsymbol{R}_{2_{\rm S}} + |\boldsymbol{R}_{2_{\rm S}}|} \right), \quad (5)$$

where the position vectors of the two stations, $\boldsymbol{R}_{1_{\rm S}}$ and $\boldsymbol{R}_{2_{\rm S}}$, are with respect to the Sun. Just as in the computation of gravitational light bending in the angle-variable case, equation (5) can be easily generalized to gravitating bodies other than the Sun; the total differential gravitational delay is found by summing over all the gravitating bodies relevant for a particular observational geometry and accuracy.

For an observed body within the solar system, equations (4) and (5) must be modified. For such an object we can compute $\boldsymbol{K}'$, its barycentric position vector corrected for light time, as in § 3. The corresponding position vectors of the observed body with respect to the Sun and stations 1 and 2 are, in our notation, $\boldsymbol{K}'_{\rm S}$, $\boldsymbol{K}'_{R_1}$, and $\boldsymbol{K}'_{R_2}$, respectively. Equation (4) is based on plane wave fronts, but for solar system bodies the wave fronts are spherical, with center at position $\boldsymbol{K}'$. The first-order delay, the factor $-\boldsymbol{k}\cdot\boldsymbol{B}(t_1)/c$ in the numerator of equation (4), is effectively replaced by $[\,|\boldsymbol{K}' - \boldsymbol{R}_2(t_1)| - |\boldsymbol{K}' - \boldsymbol{R}_1(t_1)|\,]/c$ (for a complete development, see Sovers & Jacobs 1996). As we will see, for the purposes of this paper this effect is irrelevant, but the generalization of equation (5) for bodies of finite distance is not. Using the development given in Hellings (1986), we obtain

$$\Delta t_g = (1+\gamma)\frac{GM_\odot}{c^3} \times \left[\ln\left(\frac{\boldsymbol{k}'_{R_1}\cdot\boldsymbol{R}_{1_{\rm S}} + |\boldsymbol{R}_{1_{\rm S}}|}{\boldsymbol{k}'_{R_2}\cdot\boldsymbol{R}_{2_{\rm S}} + |\boldsymbol{R}_{2_{\rm S}}|} \right) + \ln\left(\frac{\boldsymbol{k}'_{R_2}\cdot\boldsymbol{K}'_{\rm S} + |\boldsymbol{K}'_{\rm S}|}{\boldsymbol{k}'_{R_1}\cdot\boldsymbol{K}'_{\rm S} + |\boldsymbol{K}'_{\rm S}|} \right) \right], \quad (6)$$

where $\boldsymbol{k}'_{R_1}$ and $\boldsymbol{k}'_{R_2}$ are the unit vectors corresponding to position vectors $\boldsymbol{K}'_{R_1}$ and $\boldsymbol{K}'_{R_2}$.

Furthermore, because equation (5) is the result of a first-order development (straight-line photon trajectories), it requires an additional term for sources observed close to the Sun. This term, as given in the IERS documents, for sources at infinity is

$$\delta t_g = (1+\gamma)^2\frac{G^2M_\odot^2}{c^5}\frac{\boldsymbol{B}(t_1)\cdot(\boldsymbol{r}_{1_{\rm S}} + \boldsymbol{k})}{(\boldsymbol{k}\cdot\boldsymbol{R}_{1_{\rm S}} + |\boldsymbol{R}_{1_{\rm S}}|)^2}, \quad (7)$$

where $\boldsymbol{r}_{1_{\rm S}}$ is the unit vector corresponding to $\boldsymbol{R}_{1_{\rm S}}$. The quantity δt_g is added to Δt_g from equation (5). Equation (7) also can be applied with small error to sources in the outer solar system if $\boldsymbol{k}$ is replaced by $\boldsymbol{k}'_{R_1}$.

5. RECONCILING THE ANGLE- AND DELAY-VARIABLE APPROACHES

Reconciling the angle- and delay-based algorithms is based on a simple construction. We compute the geometric direction of a star (infinitely distant) from a given point $\boldsymbol{R}_1$ on the surface of Earth; the spherical coordinates are (α, δ). That is, using the notation of § 3, we start with the unit vector $\boldsymbol{k}'_{R_1}$, which, for objects at infinity, is the same as $\boldsymbol{k}$. Suppose we have an aperture plane orthogonal to $\boldsymbol{k}'_{R_1} = \boldsymbol{k}$, passing through point $\boldsymbol{R}_1$, with the maximum linear dimension of the aperture small compared with the radius of Earth.

Within the traditional paradigm, the effects of the gravitational deflection of light and aberration shift the apparent direction of the object to $\boldsymbol{k}'''_{R_1}$. That is, in the topocentric frame of our aperture the wave fronts come from the direction $\boldsymbol{k}'''_{R_1}$, and there will be a linear gradient of phase across the aperture. If the aperture is a focusing element, this phase gradient produces, in the image plane, an offset of the point-spread function (PSF) from the optical axis. Assuming that we can point the aperture as precisely as needed, the offset of the PSF from the optical axis can be measured, yielding the differential angular coordinates ($\Delta\alpha$ and $\Delta\delta$) of the apparent position of the object relative to its geometric position. We can thus measure the effects of gravitational light bending and aberration using a more or less direct measurement of angle.

From another point of view, however, our aperture can be regarded as simply an array of infinitesimal surface elements, any two of which are separated by a vector that can be thought of as an interferometer baseline. An interferometric delay can (in principle) be measured for each such baseline, directly sampling, at two points, the phase gradient across the aperture. In the topocentric frame, the phase gradient results from the apparent tilt of the wave fronts with respect to the aperture plane. As previously noted, for connected-element interferometers, the delay is usually computed using the angle between the baseline and the apparent direction of the star. However, we can also take the geocentric VLBI approach and compute the delay without using any angles measured in the local frame.

The approach used here is to apply one of the VLBI delay algorithms to two orthogonal baselines, $\boldsymbol{B}_r$ and $\boldsymbol{B}_d$, which are part of the small aperture and thus orthogonal to $\boldsymbol{k}'_{R_1} = \boldsymbol{k}$. The two baselines are of equal length B, with baseline $\boldsymbol{B}_r$ pointing in the direction of increasing right ascension and $\boldsymbol{B}_d$ pointing in the direction of increasing declination. The baselines have the point $\boldsymbol{R}_1$ as their common origin, with the points at the opposite ends designated $\boldsymbol{R}_{2r}$ and $\boldsymbol{R}_{2d}$, respectively (see Fig. 1). These two baselines, together with the unit vector $\boldsymbol{k}$, effectively define an orthogonal basis for a spherical polar (curvilinear) coordinate system at $\boldsymbol{R}_1$. This construction allows us to immediately transform the computed delay values for the two baselines to angular offsets

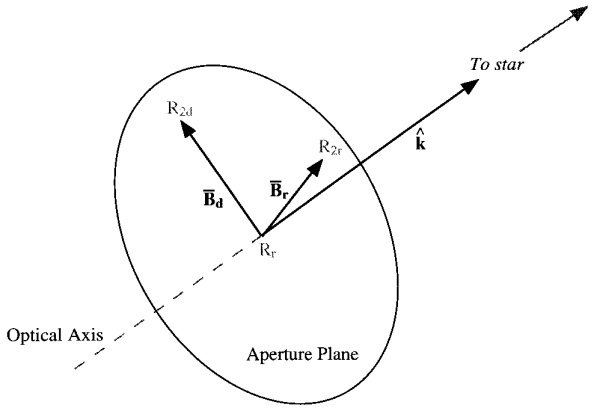

FIG. 1.—Geometry of baselines used in application of VLBI delay algorithms. The baselines $\boldsymbol{B}_r$ and $\boldsymbol{B}_d$ are in the direction of increasing right ascension and declination, respectively, as viewed from the common point $\boldsymbol{R}_1$. Both baselines lie in the aperture plane that is orthogonal to $\boldsymbol{k}$, which points in the star's geometric direction.

$\Delta\alpha$ and $\Delta\delta$, since either delay divided by B/c is the direction cosine of the apparent stellar position with respect to the baseline direction.

However, for the apparent position of the star computed in such a way to be comparable to that computed from the traditional approach, it must be expressed in the topocentric frame of the aperture. That is, the delay values must be expressed in what is essentially local proper time. Since VLBI delay algorithms yield delay values for a geocentric frame, some modification of the algorithms is required. Fortunately, because in our construction $\boldsymbol{B}_r$ and $\boldsymbol{B}_d$ are orthogonal to $\boldsymbol{k}$, some simplifications also arise. For example, for our application, the VLBI delay algorithm represented by equation (4) becomes

$$\tau_{R_1} = \frac{\Delta t_g - [\dot{\boldsymbol{R}}_1 \cdot \boldsymbol{B}(t_1)/c^2](1 + \boldsymbol{k} \cdot \dot{\boldsymbol{R}}_1/2c)}{1 + (\boldsymbol{k}/c) \cdot (\dot{\boldsymbol{R}}_1 + \dot{\boldsymbol{R}}_{2_{R_1}})} . \quad (8)$$

The first term in square brackets in equation (4) does not appear in equation (8), since $\boldsymbol{k} \cdot \boldsymbol{B}(t_1) = 0$. Equation (8) yields the delay in local time, because it uses the barycentric velocity of our basic reference point, $\dot{\boldsymbol{R}}_1$, in place of the barycentric velocity of the geocenter, $\dot{\boldsymbol{E}}$. Similarly, the velocity of opposite end of the baseline is now measured with respect to $\dot{\boldsymbol{R}}_1$ instead of the geocenter, that is, $\dot{\boldsymbol{R}}_{2_{R_1}}$ has replaced $\dot{\boldsymbol{R}}_{2_E}$. (Point $\boldsymbol{R}_2$ can represent either $\boldsymbol{R}_{2r}$ or $\boldsymbol{R}_{2d}$, depending on which baseline's delay is being computed.) Note that the vector sum $\dot{\boldsymbol{R}}_1 + \dot{\boldsymbol{R}}_{2_{R_1}}$ in the denominator is equal to the barycentric velocity of station 2, just as is the corresponding sum in equation (4).

No changes are required in equation (5) or (6), since these equations, standing alone, apply to the barycentric reference system. The quantity $\Delta\tau_g$ is transformed into the geocentric or topocentric system by the action of the denominator in equation (4) or (8), respectively.

Other VLBI delay algorithms can be used in the same way and tested against the angle-variable algorithms. The Soffel et al. (1991) algorithm reduces to, for the case at hand,

$$\tau_{R_1} = \Delta t_g - \frac{1}{c^2} [\dot{\boldsymbol{R}}_1 \cdot \boldsymbol{B}(t_1)] \times \left[1 - \frac{1}{2c} (\boldsymbol{k} \cdot \dot{\boldsymbol{R}}_1) - \frac{1}{c} (\boldsymbol{k} \cdot \dot{\boldsymbol{R}}_{2_{R_1}})\right] . \quad (9)$$

The Hellings (1986) algorithm reduces to an even simpler form:

$$\tau_{R_1} = \Delta t_g - \frac{1}{c^2} [\dot{\boldsymbol{R}}_1 \cdot \boldsymbol{B}(t_1)]\left[1 + \frac{1}{2c} (\boldsymbol{k} \cdot \dot{\boldsymbol{R}}_1)\right] . \quad (10)$$

Hellings also presents a slightly different form of the equation for the gravitational delay for an object at infinity:

$$\Delta t_g = -(1 + \gamma) \frac{GM_\odot}{c^3 R_{1_S}} \left[\frac{(\boldsymbol{k} + \boldsymbol{r}_{1_S}) \cdot \boldsymbol{B}(t_1)}{1 + \boldsymbol{k} \cdot \boldsymbol{r}_{1_S}}\right] , \quad (11)$$

where, if $\boldsymbol{R}_{1_S}$ is a vector from the Sun to the observer, then R_{1_S} is its length and $\boldsymbol{r}_{1_S}$ is the corresponding unit vector.

Finally, we must consider why, as previously asserted, we can ignore spherical wave front effects for solar system objects. The effects we are interested in here are linear in baseline length for short baselines. This linearity means that the local angle we obtain from the delay value is constant over a wide range of baseline lengths. However, the extra delay component due to the sphericity of wave fronts from solar system objects is quadratic in baseline length. Therefore, by reducing the size of our hypothetical aperture sufficiently, we can make the delay component due to wave front curvature negligible relative to the delay component from the effects of interest. From another perspective, we have limited ourselves to two baselines because that is the minimum needed to determine an apparent direction in two dimensions. If we were to use more baselines, then the ensemble of delay values would allow us to easily solve for and remove the delay component due to wave front curvature. Therefore, for present purposes, wave front curvature can be ignored and equations (8)–(10) used for solar system objects by merely replacing $\boldsymbol{k}$ with $\boldsymbol{k}'_{R_1}$.

6. NUMERICAL EXPERIMENTS

The angle-variable and VLBI algorithms were quantitatively compared by numerically implementing the strategy outlined in § 5 for a group of celestial objects. That scheme allows us to generate, from whatever VLBI algorithm is to be tested, a topocentric apparent place—an angular position in the reference frame of the small aperture. This position can then be compared with a traditional apparent place computed using the angle-variable algorithms described in § 3.

Software was written to evaluate the reduced form of the three VLBI delay algorithms: the IERS algorithm (eq. [8]), the Soffel et al. algorithm (eq. [9]), and the Hellings algorithm (eq. [10]). In the IERS and Soffel et al. algorithm implementations, equation (6) was used for $\Delta\tau_g$ for both stars and solar system objects; it reduces to equation (5) for objects at infinity. In the Hellings algorithm implementation, equation (11) was used for $\Delta\tau_g$ and the analysis was limited to stars. The algorithms were applied to two equal-length baselines orthogonal to each other and the geometric direction of the object, as described in § 5 and shown in Figure 1. The length of these baselines was an input variable, typically in the range 1–100 m. Once the two delays were computed, they were converted to $\Delta\alpha$ and $\Delta\delta$ values as described in § 5; these were added to the coordinates (α, δ) of the geometric direction of the object to form a "VLBI apparent place."

The software also evaluated, for the same object, the topocentric angular position as affected by the gravitational deflection of light and aberration, computed using the

angle-variable algorithms given in § 3. Subroutines from the NOVAS astrometric package (Kaplan 1990) were used, which directly provide an apparent place of the object of interest. This apparent place was then compared to the VLBI apparent place. Differences were formed in α, δ, and arc.

Some of the details of this software should be mentioned. First, the gravitational deflection of light was computed using only the Sun's field, since adding in the smaller effects of other bodies—Jupiter or Earth, for example—does not provide any information about the correctness of the basic algorithm. Second, precession and nutation, which are simply rotations of the reference frame, were not applied at any point. All coordinates were therefore with respect to the equator and equinox of J2000.0. Third, for solar system objects, light time was computed using the procedure outlined in § 3 for both the angle-variable and VLBI algorithms. (Note that for the purposes of this paper, light time could have been omitted entirely.)

To ensure that the angle-variable algorithms from § 3 were correctly implemented, results from the NOVAS code were compared with results from the corresponding code from the SLALIB package (Wallace 1994). When the same solar system ephemeris data were used in the calculations, the differences in star positions were at the 10^{-10} arcsec level, which is numerical noise for angular values represented in IEEE double-precision floating-point format.

Attention was also given to the potential numerical problems of computing the VLBI delay for a very short baseline. Difficulties can arise because of the near-equality of the quantities $\boldsymbol{R}_{1\mathrm{S}}$ and $\boldsymbol{R}_{2\mathrm{S}}$ in equations (5) and (6), as well as the near-equality of $\boldsymbol{k}'_{R_1}$ and $\boldsymbol{k}'_{R_2}$ in equation (6). If IEEE double-precision floating-point arithmetic is used, then $\boldsymbol{R}_{1\mathrm{S}}$ and $\boldsymbol{R}_{2\mathrm{S}}$ are represented to about 15 decimal digits of precision. These vectors are heliocentric, and if the two positions they represent are 10 m apart, the first 10 digits of the corresponding components of the two vectors will be the same, leaving only five digits of precision for the difference between them. Similar considerations hold for $\boldsymbol{k}'_{R_1}$ and $\boldsymbol{k}'_{R_2}$. Equations (5) and (6) account for the effect of the Sun's gravitational field, which, in angular terms, is greater than 0.″1 within 5° of the Sun. Therefore, near the Sun we would expect numerical errors to appear at about the 10 μas level. In early testing of the algorithm comparison, this was observed. There are several strategies to avoid these errors. One is to simply limit our comparison to longer baselines or greater elongations. Another is to expand equations (5) and (6) in small quantities; for example, equation (11) results from an expansion of equation (5) in $\boldsymbol{B} = \boldsymbol{R}_{2\mathrm{S}} - \boldsymbol{R}_{1\mathrm{S}}$. However, a first-order formula of this sort is not sufficiently accurate. A more general and easily implemented solution (if less elegant) is to simply use more numerical precision. Therefore, equation (6) was implemented in extended-precision (31 digit) arithmetic to avoid the numerical degeneracy. The success of this approach depends to some degree on how the vectors involved are constructed, since the basic solar system ephemerides are represented only in double-precision floating-point words.

Each algorithm comparison was performed for 16,471 imaginary stars distributed around the celestial sphere at 2° intervals of α and δ. A separate set of comparisons was made within 15° of the Sun, where the imaginary stars were at $\frac{1}{3}$° intervals (beyond the solar limb). The proper motions and parallaxes of these stars were assumed to be zero. Comparisons were also performed for selected planets, using barycentric coordinates obtained from the JPL DE200 ephemeris (Standish 1990). The planetary positions were computed at half-day intervals over the 4 year period beginning at 1995.0. For both the star and planet computations, the barycentric position and velocity of Earth were also obtained from DE200. The results from all of the computer runs are described in the following section.

7. RESULTS AND DISCUSSION

For each VLBI algorithm that was tested, several types of plots were generated. All-sky maps were produced that use the shading at each point on the map to indicate the arc difference between the VLBI apparent place and the conventional apparent place, for an infinitely distant star at that point. Maps showing the more densely sampled region near the Sun were also generated. Supplementing these maps were "flow diagrams" that showed the direction of the differences between the algorithms across the sky. In addition, for the Soffel et al. and IERS algorithms, plots were produced showing the difference between the VLBI apparent place and the conventional apparent place of selected planets as a function of time. For the planet plots, the algorithm differences in right ascension, declination, and arc were plotted. Statistical data on the comparison were also generated for each plot.

Although each of the all-sky maps was computed for a specific geographic location and date, it was found that the overall pattern of the algorithm differences on the sky, with respect to the position of the Sun and the ecliptic, did not vary significantly with time or place. Similarly, the planet plots appeared to be insensitive to the observer's location; however, if an extended span of time was plotted, the curves were seen to repeat with the synodic period of the planet. The algorithm differences also did not depend on baseline length for baselines ≤ 1 km, although numerical noise began to appear below the microarcsecond level for these short baselines (the long-baseline case is discussed in § 8). A selection of the most revealing of the ensemble of plots is shown as Figures 2–6, and their interpretation is described below. Unless otherwise noted, all the plots used here were computed for longitude -120° and latitude 30°, using 100 m VLBI baselines. The all-sky maps for the stellar case were computed for 1996 May 1 at 0000 TT, while the planet plots covered the years 1995 through 1998.

Figure 2 shows the all-sky difference map for the Hellings algorithm. The positions of the Sun, the ecliptic pole, and the apex of the observer's instantaneous velocity are marked. The shading is linear in the arc difference between algorithms, with the black-to-white range representing differences of 0–1 mas. The figure indicates a major difference between the Hellings and angle-variable algorithms that must be associated with aberration, since maxima occur in two rings, 45° and 135° from the velocity apex. Furthermore, the direction of the difference at each point (not shown in the figure) is aligned directly toward or away from the velocity apex. However, the largest differences between the Hellings and angle-variable algorithms actually occur very close to the Sun (within the width of the Sun symbol on the map) and reach 16 mas.

Differences between algorithms at such levels is significant for modern astrometric applications. The Hellings VLBI algorithm is a decade old, however, and its design specification was "tenths of a nanosecond" in delay. As a

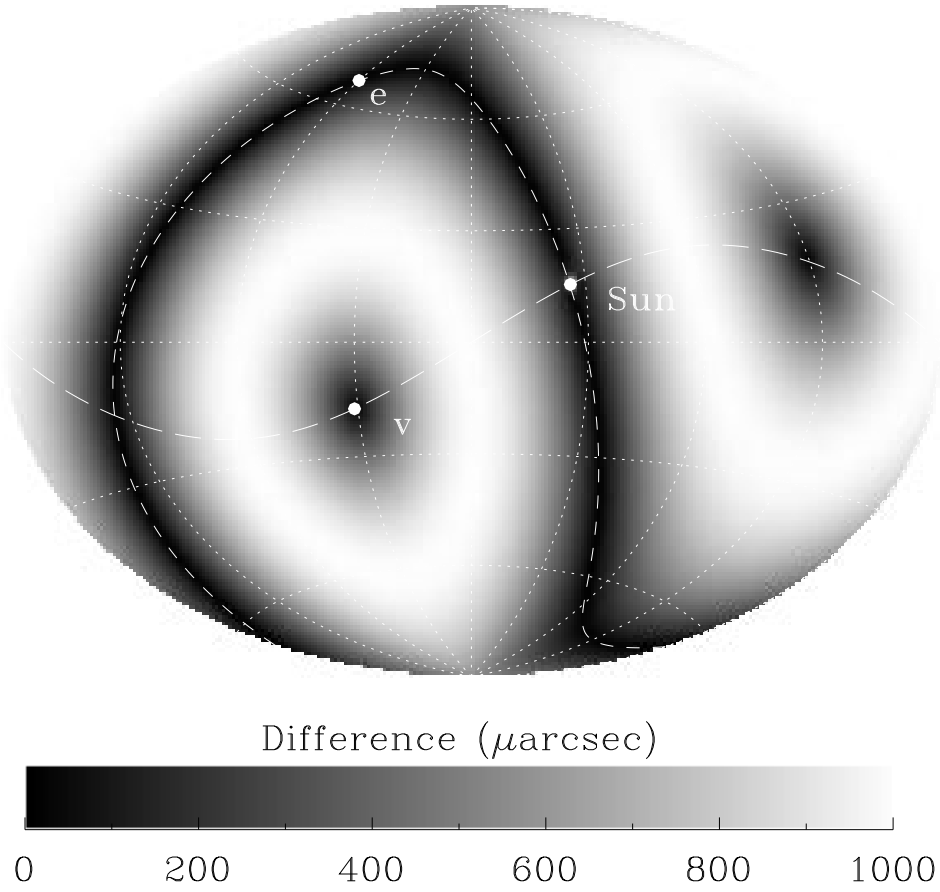

FIG. 2.—All-sky map showing the arc differences between star positions computed using the Hellings VLBI delay algorithm and the standard angle-variable algorithms used in optical astrometry. These computations used a grid of artificial stars at infinity and 100 m VLBI baselines. The black-to-white shading range represents differences of 0–1 mas. The positions of the Sun, the ecliptic pole (e), and the apex of the observer's instantaneous velocity (v) are indicated. The long-dashed curve is the ecliptic, and the short-dashed curve is 90° from the velocity apex.

fraction of the maximum delay of $a_E/c = 0.021$ s for ground-based interferometers (where a_E is the Earth radius), ± 0.1 ns in delay accounts for the 1 mas difference in apparent position that we see over most of the sky (at least in magnitude) and does not require that any error be assigned to the conventional angle-based algorithms. The situation close to the Sun is not as clear, although the Hellings gravitational delay formula is an approximation to those used in the later VLBI algorithms. Improvements were made to the Hellings VLBI model by Shahid-Saless et al. (1991).

The Soffel et al. algorithm provides a more interesting case. It was designed for picosecond delay accuracy; ± 1 ps translates to about 10 μas in apparent place. Figure 3 shows the difference maps for this algorithm, computed and presented in the same manner as Figure 2. In Figure 3, however, the differences between the VLBI and angle-based algorithms are 3 orders of magnitude smaller than those in Figure 2, with the shading range representing 0–0.75 μas differences. Since the angle-based algorithms have not been changed, the vast improvement must come from the better VLBI delay model. The pattern shown in Figure 3 indicates that, although the maximum differences are clearly related to the Sun (they reach ~ 2 μas near the solar limb), some other factor is involved that is associated with the ecliptic. The differences must result from some kind of interaction between gravitational light bending and aberration that is not identically handled in the angle-based and VLBI algorithms.

Figure 4 is the difference map for the IERS algorithm, and we see another order-of-magnitude improvement; here the shading range represents only 0–0.025 μas differences. Over most of the sky, we are left with a featureless map of very low-level discrepancies, typically tens of nanoarcseconds, associated with the aberration calculations. Within a few degrees of the Sun, where gravitational light bending is greatest, the differences increase but remain below 1 μas. T. M. Eubanks (1995, private communication) has noted that the primary difference between the Soffel et al. and IERS algorithms is a Lorentz factor arising from the observer's velocity that is applied to the gravitational delay in the latter theory (denominator in eqs. [4] and [8]) but not the former. (The counterpart in the angle-based algorithms is that the gravitational deflection is computed before aberration.) This, then, explains the difference pattern seen in Figure 3 that is not present in Figure 4. Clearly, the IERS algorithm is superior to the other two VLBI algorithms, at least for objects at infinity. Table 1 numerically summarizes the results for the set of comparisons described above.

Figures 5 and 6 show the arc difference between the VLBI and angle-based computed positions for two planets, Venus and Mars, as a function of time. Figure 5 is based on the Soffel et al. algorithm and Figure 6 is based on the IERS algorithm, both with the gravitational delay formula generalized to work for objects at all distances. These plots were computed for the same geographic location and baseline length (100 m) as the previous figures. Like Figures 3 and 4,

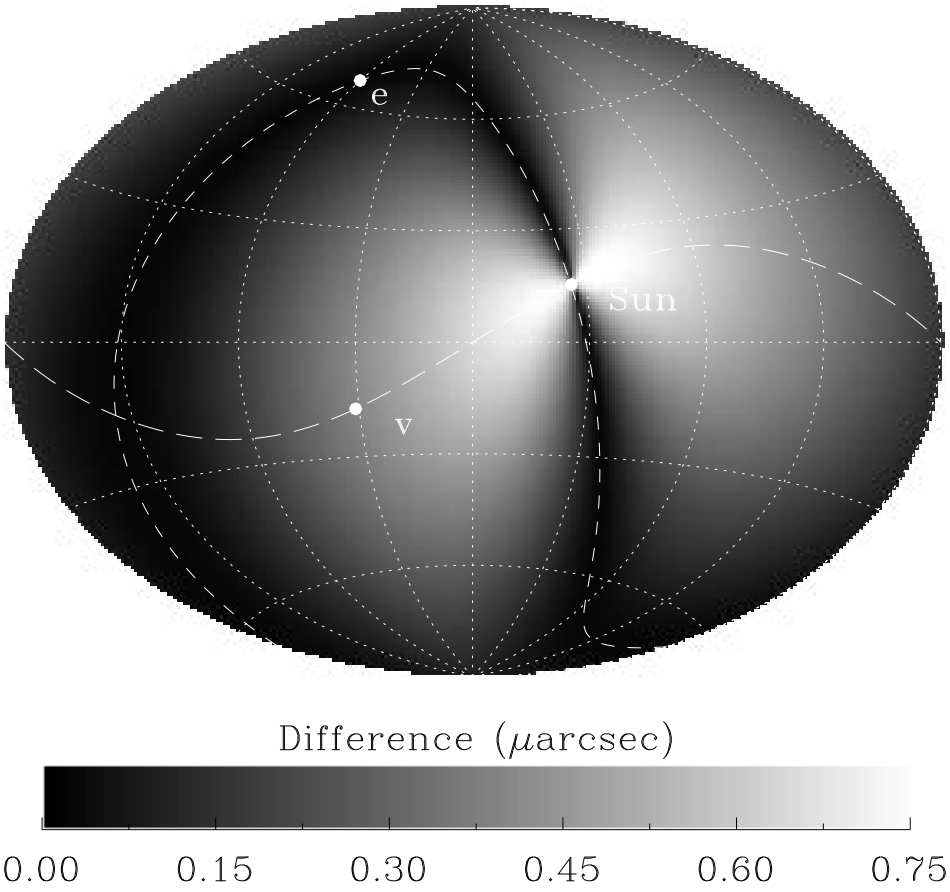

FIG. 3.—Same as Fig. 2, except that the Soffel et al. VLBI delay algorithm was used and the shading range represents differences of 0–0.75 μas

they show that the VLBI and angle-based algorithms compare quite well, with the IERS algorithm significantly better than the Soffel et al. algorithm most of the time. Differences between the IERS and angle-based algorithms remain well below 1 μas except for a forest of numerical noise spikes and some broader, more significant peaks. These peaks, which reach about 10 μas near the times when one of the planets is at conjunction with the Sun, are the counterparts to the difference maxima near the Sun that arose in the stellar computations. The exceptional peak for Mars at conjunction in 1998 occurs when Mars is occulted by the Sun.

The results described above illustrate the improvements in precision that accompanied the development of a consensus VLBI delay algorithm. Widely accepted angle-variable algorithms were already in place when this development began, and the analysis described here indicates that the confidence placed in the angle-variable algorithms was not unfounded. The small differences between the two regimes that remain may, of course, be due to either the delay- or angle-based formulations; a better version of one or the other would be needed to resolve the issue. In the next section, the comparison approach used here is exploited to test an experimental improvement made in the angle-based algorithms.

8. TESTING AN IMPROVEMENT TO THE MODEL

In the VLBI and angle-based algorithms tested so far, the general relativistic effect of the Sun's gravitational field has been derived from a first-order geometric model. That is, the total effect has been derived from a line integral over a photon trajectory that is a straight line in Euclidean space. For most trajectories (most of the sky), this is a reasonable and highly accurate approximation. However, as noted in § 4, for VLBI observations close to the Sun, a delay correction has been developed (reproduced here as eq. [7]) that accounts for path curvature. As noted by Eubanks (1991b), since the actual photon path is concave toward the Sun, the impact parameter of the ray with respect to the Sun is actually greater than in the linear approximation. For an

TABLE 1

DIFFERENCES BETWEEN VLBI AND ANGLE-VARIABLE ALGORITHMS

VLBI Algorithm	Average Difference over Whole Sky	Average Difference within 15° of Sun	Maximum Difference near Solar Limb
Hellings 1986	6.5×10^{-4}	2.5×10^{-4}	1.6×10^{-2}
Soffel et al. 1991.....	2.2×10^{-7}	4.9×10^{-7}	1.5×10^{-6}
IERS 1996	1.8×10^{-8}	2.3×10^{-8}	2.3×10^{-7}

NOTE.—In units of arcseconds.

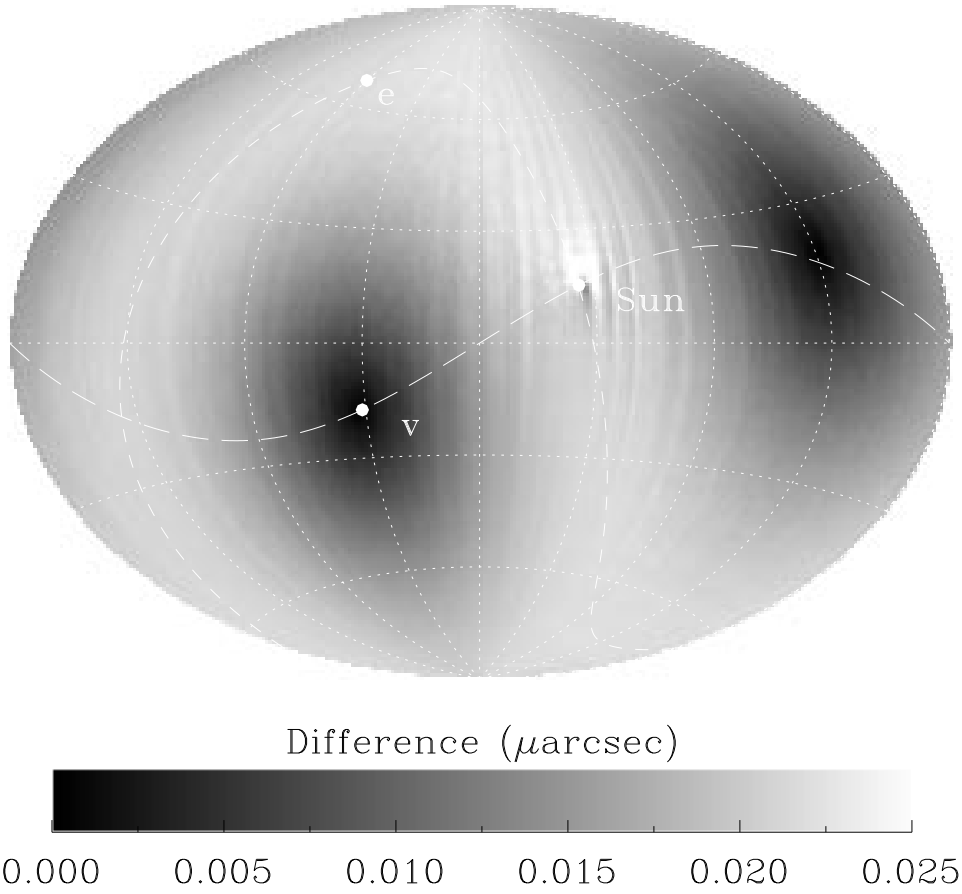

FIG. 4.—Same as Fig. 2, except that the IERS VLBI delay algorithm was used and the shading range represents differences of 0–0.025 μas

object at infinity observed on Earth, this tends to lessen the total gravitational delay and the apparent angular deflection of the photon's path. Detailed expressions for the total effect, including high-order terms, have been presented by Richter & Matzner (1982, 1983), whose work formed the basis for the VLBI delay correction given in the IERS documents and here.

We can include the path-curvature VLBI delay correction (eq. [7]) in the IERS algorithm and again compute the differences with the standard angle-based algorithms. (Referring to this as a path-curvature correction, rather than as a second-order correction, avoids nomenclatural confusion with terms in the relativistic metric.) Averaged over the whole sky, the differences increase by 44%, but most of the effect is concentrated near the Sun, where the differences reach a few milliarcseconds. Apparently, this is an indication of the error in the standard algorithm for angular deflection due to neglect of path curvature.

An approximate path-curvature correction was then applied to the angular deflection algorithm. Equation (1)

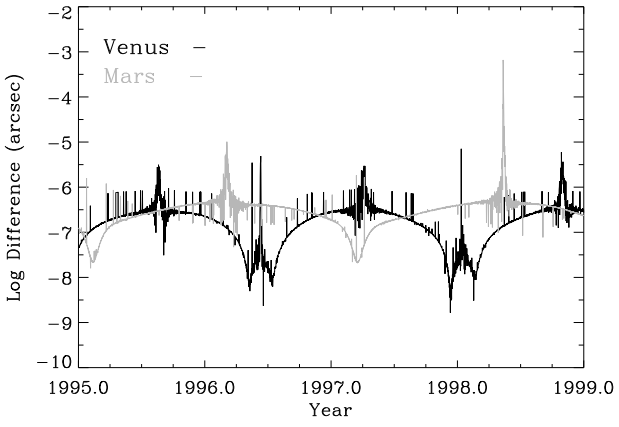

FIG. 5.—Differences between planet positions computed using the Soffel et al. VLBI delay algorithm and the standard angle-variable algorithms used in optical astrometry. Differences for Venus are shown in black, and those for Mars are shown in gray. This comparison required that the usual VLBI formula for differential gravitational (Shapiro) delay be generalized for use with solar system objects.

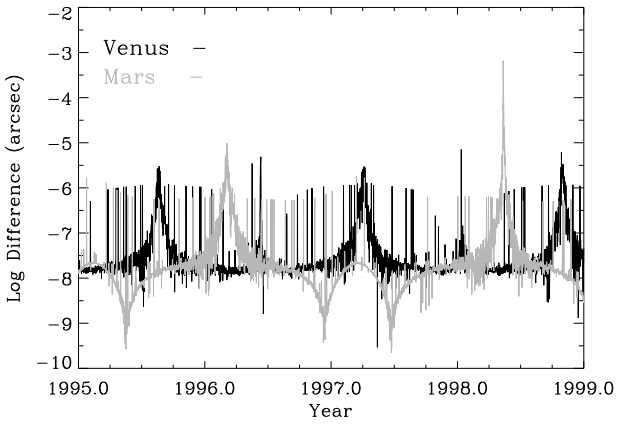

FIG. 6.—Same as Fig. 5, except that the IERS VLBI algorithm was used. Note that the difference "floor" is lower by about an order of magnitude, making this plot appear noisier than Fig. 5.

TABLE 2

ALGORITHM DIFFERENCES AS A FUNCTION OF BASELINE LENGTH

Baseline Length (km)	Average Difference over Whole Sky	Average Difference within 15° of Sun	Maximum Difference near Solar Limb
1	1.7×10^{-8}	4.0×10^{-8}	1.5×10^{-5}
10	1.6×10^{-8}	4.6×10^{-8}	1.4×10^{-5}
100	1.8×10^{-7}	6.4×10^{-7}	1.8×10^{-4}
1000	1.9×10^{-6}	6.6×10^{-6}	1.9×10^{-3}
10000	1.9×10^{-5}	5.6×10^{-5}	1.9×10^{-2}

NOTE.—In units of arcseconds.

was recast so that the undeflected impact parameter of the ray appears as a variable in the denominator. Let the magnitude of the deflection given by equation (1) be $\Delta\phi$ and the observer-Sun distance be R_S. The correction scheme is simply to increase the impact parameter of the ray by $R_S\Delta\phi$ and recompute the gravitational deflection using the new impact parameter. When the results of this new angular deflection algorithm are compared with those from the improved VLBI delay model, the large differences between the two regimes near the Sun are reduced by an order of magnitude, and the all-sky average reverts to the value obtained from the comparison of the two original algorithms. The two algorithms with the path-curvature corrections produce a difference map that is indistinguishable from Figure 4. (Neither of the path-curvature corrections is valid for observations of solar system bodies, although in both cases the error would be small for objects in the outer solar system.) It is rather surprising that the crude correction applied to the standard angle-based algorithm works so well, but the results show the value of directly comparing independently derived algorithms for two different observing domains. Obviously, if higher angular accuracy is needed close to the Sun, the next step would be to implement a true high-order gravitational bending algorithm based on, for example, the Richter & Matzner (1982) or Klioner & Kopejkin (1992) developments.

9. THE LARGE-APERTURE CASE

The form of the VLBI delay algorithms that we have been using is a special case that applies to baselines orthogonal to the geometric direction of the object and delay measured in the proper time of station 1. However, no conditions or approximations were introduced based on the distance between the two stations, so the VLBI algorithms used here

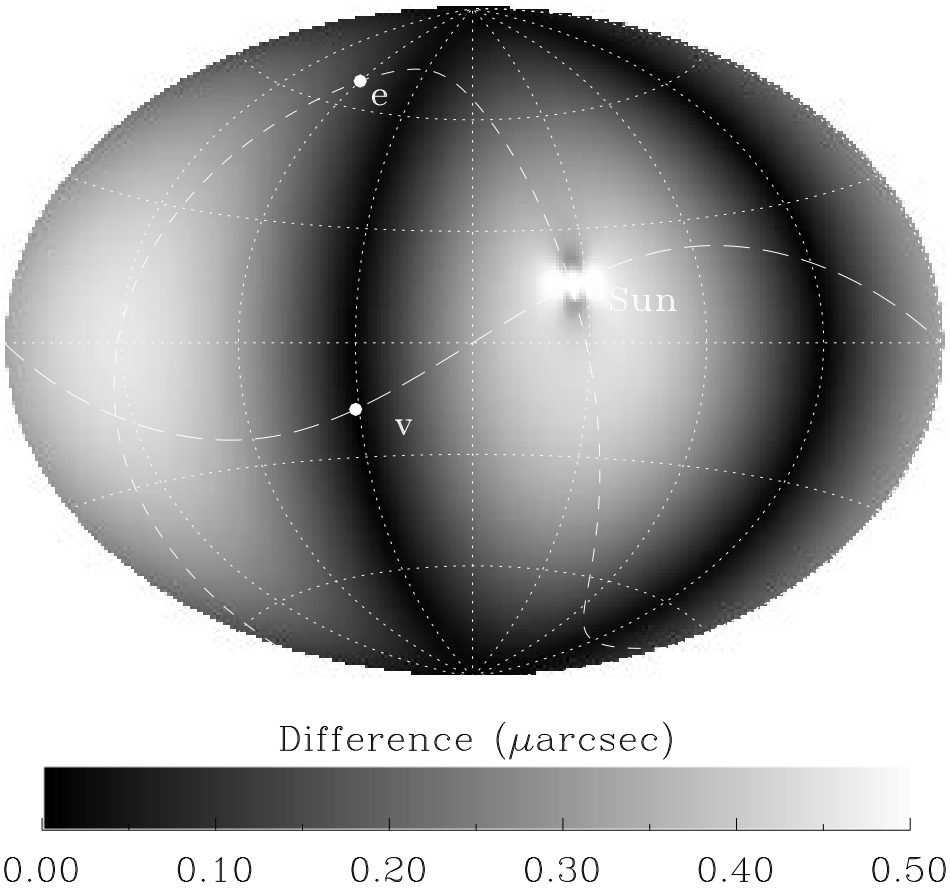

FIG. 7.—Same as Fig. 4, except that the VLBI baselines used were 100 km long. The shading range represents differences of 0–0.5 μas.

should remain valid for baselines up to $\sim 10^7$ m. In contrast, the angle-variable algorithms have been derived for a single-point observer and do not contain any variable that relates to aperture size. Using the technique described in §§ 5 and 6, we can compare the two kinds of algorithms on increasingly long VLBI baselines and obtain the error that results from applying the angle-variable algorithms to instruments with large apertures.

Comparisons of the VLBI and angle-based algorithms were made for a series of VLBI baseline lengths. For this series of comparisons, the algorithms used were those described in § 8, which included the path-curvature gravitational delay/bending corrections. The results for baselines shorter than a few kilometers are not significantly different from those reported in § 8 for the 100 m baseline. For 10–10,000 km baselines, the differences between the VLBI and angle-based algorithms increase linearly with baseline length but remain small. Table 2 summarizes the results from a typical series of computations. Table 2 reflects, for the geometry that we are using, the weak nonlinearity of VLBI delay as a function of baseline length (sometimes referred to as "relativistic parallax"). For the 100 km baseline case, the differences between the angle- and delay-based algorithms as they map onto the sky are shown in Figure 7, where the black-to-white shading range represents 0–0.5 μas differences (cf. Fig. 4). Interestingly, the differences that emerge are all in right ascension.

The angle-based algorithms seem to be quite good even for very large apertures. However, this set of tests applies only to the normal way in which these algorithms are applied in optical astrometry, which is to an object on a line of sight orthogonal to the aperture plane. A different kind of test would be required to provide information on whether a large interferometer such as, for example, the VLA, could use the angle-based and delay-based algorithms interchangeably for all observing geometries. The tests described above answer that question only for sources observed at the zenith.

10. CONCLUSION

This paper has presented information on the correspondence between algorithms used in two astrometric regimes: the optical regime, where the observables are angular quantities, and the VLBI radio regime, where the interferometric group delay is the observable. The physical effects that the algorithms of interest account for are relativistic aberration and gravitational light deflection (in the language of angular variables). A procedure was presented by which VLBI algorithms can be used to generate angular positions that can be compared with those computed using the standard optical algorithms. The software developed for this, called WAAAV (Wide-Angle Astrometry Algorithms from VLBI), is available from the author.

This software has been used to quantitatively evaluate the differences between the algorithms used in the two regimes. This analysis showed that the VLBI algorithms have become substantially more sophisticated over the last decade and that the VLBI and optical algorithms now correspond at the microarcsecond level or better over most of the sky. Furthermore, the analysis demonstrates that the optical algorithms can be applied in the usual way to very large apertures, without significant error.

The correspondence between these algorithms provides information on their *precision*, which, as used here, refers to how well a physical model is embodied in the mathematics used to account for it. Historically, the developments of the optical and radio algorithms used the same physical model, based on special and general relativity, but progressed along separate mathematical paths. What has not been addressed is the *accuracy* of these algorithms, that is, how well the physical model corresponds to reality. Ultimately, of course, this can only be determined by actual observation. However, it is well known that these algorithms, as usually implemented, are not accurate at the microarcsecond level of precision reported here—a level that could soon be important observationally.

The incompletenesses in the algorithms fall into two categories. The first arises from the way in which the algorithms are implemented in software. Often, for example, gravitational deflection is evaluated only for the Sun, as was done for the comparisons reported in this paper. Yet Jupiter's mass is 10^{-3} that of the Sun, and its effects are greater than 1 μas over almost half the celestial sphere; Saturn's effect is one-sixth as great. Earth's field adds a deflection of order 0.1 mas over most of the sky. Furthermore, in computing gravitational deflection, the position of the gravitating body changes over the photon's time of flight, an effect that Shahid-Saless et al. (1991) treat. At the very least, the deflection should be computed using the position that the gravitating body had when the observed photons passed closest to it. Analogous statements could be made about gravitational delay.

A more important category of algorithm incompleteness is in the fundamental mathematical expressions, which do not always account for all of the significant physics. In addition to the path-curvature corrections to gravitational deflection/delay described in § 8, there are higher order terms for spherical gravitational fields and terms for the effects of nonspherical gravitational fields—the quadrupole component and the dipole gravitometric component for rotating bodies. These effects have been described by Richter & Matzner (1982, 1983), Brumberg, Klioner, & Kopejkin (1990), Klioner & Kopejkin (1992), and Páez & Frutos (1994). Over most of the sky they are quite small, but they can be significant at the microarcsecond level or greater near the limbs of solar system bodies. In addition, more theoretical work is needed on the validity of the simple addition of gravitational deflections or delays from separate bodies and the use of constants and measurements (such as station and planetary coordinates) that are not necessarily all expressed in the same metric.

Perhaps the principal value of the algorithm comparison scheme described in this paper is its utility in validating these kinds of extensions to the underlying physical model. The example presented in this paper was the addition of path-curvature corrections to the gravitational deflection/delay algorithms. Independently derived corrections were introduced into the delay-based and angle-based algorithms and the results compared. The small numerical differences that resulted when the corrections were used in both regimes, in contrast to the much larger differences when the algorithms were mismatched, provided a measure of confidence that the corrections were at least formally sound. This example demonstrates that the development described in this paper can serve as a helpful diagnostic tool in implementing new algorithms required by increasingly sophisticated and accurate observing systems.

REFERENCES

Brumberg, V. A., Klioner, S. A., & Kopejkin, S. M. 1990, in IAU Symp. 141, Inertial Coordinate System on the Sky, ed. J. H. Lieske & V. K. Abalakin (Dordrecht: Kluwer), 229
Eubanks, T. M., ed. 1991a, Proc. US Nav. Obs. Workshop on Relativistic Models for Use in Space Geodesy (Washington: US Nav. Obs.)
———. 1991b, in Proc. US Nav. Obs. Workshop on Relativistic Models for Use in Space Geodesy, ed. T. M. Eubanks (Washington: US Nav. Obs.), 60
Fukushima, T. 1995, Highlights Astron., 10, 185
Green, R. M. 1985, Spherical Astronomy (Cambridge: Cambridge Univ. Press)
Hellings, R. W. 1986, AJ, 91, 650
Høg, E., & Seidelmann, P. K., eds. 1995, IAU Symp. 166, Astronomical and Astrophysical Objectives of Sub-Milliarcsecond Optical Astrometry (Dordrecht: Kluwer)
Hohenkerk, C. Y., Yallop, B. D., Smith, C. A., & Sinclair, A. T. 1992, in Explanatory Supplement to the Astronomical Almanac, ed. P. K. Seidelmann (rev. ed.; Mill Valley, CA: Univ. Sci.), 95
Hughes, J. A., Smith, C. A., & Kaplan, G. H., eds. 1991, IAU Colloq. 127, Reference Systems (Washington: US Nav. Obs.)
Hutter, D. J., Johnston, K. J., & Mozurkewich, D. 1995, in IAU Symp. 166, Astronomical and Astrophysical Objectives of Sub-Milliarcsecond Optical Astrometry, ed. E. Høg & P. K. Seidelmann (Dordrecht: Kluwer), 23
IAU. 1996, Trans. IAU, 22B, 47
Jacobs, C. S., & Sovers, O. J. 1993, in IAU Symp. 156, Developments in Astrometry and their Impact on Astrophysics and Geodynamics, ed. I. I. Mueller & B. Kolaczek (Dordrecht: Kluwer), 173
Johnston, K. J., et al. 1995, AJ, 110, 880
Kaplan, G. H. 1990, BAAS, 22, 930
Kaplan, G. H., Hughes, J. A., Seidelmann, P. K., Smith, C. A., & Yallop, B. D. 1989, AJ, 97, 1197
Klioner, S. A., & Kopejkin, S. M. 1992, AJ, 104, 897
Lederle, T., & Schwan, H. 1984, A&A, 134, 1
Lieske, J. H., & Abalakin, V. K., eds. 1990, IAU Symp. 141, Inertial Coordinate System on the Sky (Dordrecht: Kluwer)
Lindegren, L., et al. 1992, A&A, 258, 18
Lindegren, L., & Perryman, M. A. C. 1995, in Future Possibilities for Astrometry in Space, ed. T.-D. Guyenne (ESA SP-379) (Noordwijk: ESA), 23
Ma, C. 1990, in IAU Symp. 141, Inertial Coordinate System on the Sky, ed. J. H. Lieske & V. K. Abalakin (Dordrecht: Kluwer), 271
McCarthy, D. D., ed. 1992, IERS Standards 1992 (IERS Tech. Note 13) (Paris: Obs. Paris)
———. 1996, IERS Conventions 1996 (IERS Tech. Note 21) (Paris: Obs. Paris)
Mignard, F. 1995, in Future Possibilities for Astrometry in Space, ed. T.-D. Guyenne (ESA SP-379) (Noordwijk: ESA), 19
Murray, C. A. 1983, Vectorial Astrometry (Bristol: Hilger)
Páez, J., & Frutos, F. 1994, Ap&SS, 214, 71
Reasenberg, R. D., et al. 1988, AJ, 96, 1731
Richter, G. W., & Matzner, R. A. 1982, Phys. Rev. D, 26, 2549
———. 1983, Phys. Rev. D, 28, 3007
Robertson, D. S. 1975, Ph.D. thesis, MIT
Ryan, J. 1991, in Proc. US Nav. Obs. Workshop on Relativistic Models for Use in Space Geodesy, ed. T. M. Eubanks (Washington: US Nav. Obs.), 5
Seidelmann P. K., et al. 1995, in Future Possibilities for Astrometry in Space, ed. T.-D. Guyenne (ESA SP-379) (Noordwijk: ESA), 187
Shahid-Saless, B., Hellings, R. W., & Ashby, N. 1991, Geophys. Res. Lett., 18, 1139
Shapiro, I. I. 1964, Phys. Rev. Lett., 13, 789
———. 1967, Science, 157, 806
Soffel, M. H. 1989, Relativity in Astrometry, Celestial Mechanics, and Geodesy (Berlin: Springer)
Soffel, M. H., Müller, J., Wu, X., & Xu, C. 1991, AJ, 101, 2306
Sovers, O. J., & Jacobs, C. S. 1996, Observation Model and Parameter Partials for the JPL VLBI Parameter Estimation Software "MODEST"—1996 (JPL Publ. 83-39, revision 6) (Pasadena: JPL)
Standish, E. M. 1990, A&A, 233, 252
Wallace, P. T. 1994, SLALIB—Positional Astronomy Library (Starlink User Note 67.20) (Chilton: Rutherford Appleton Lab.)
Woolard, E. W., & Clemence, G. M. 1966, Spherical Astronomy (New York: Academic)
Zhu, S. Y., & Groten, E. 1991, in Proc. US Nav. Obs. Workshop on Relativistic Models for Use in Space Geodesy, ed. T. M. Eubanks (English transl.; Washington: US Nav. Obs.), 38